Article

Calculation of penetration distance during ship ramming in multi-year ice

Junji SAWAMURA[1], Hajime YAMAGUCHI[2], Shuki USHIO[3], Yutaka YAMAUCHI[4]

[1] Graduate School of Engineering, Osaka University, Osaka, Japan
[2] Graduate School of Frontier Sciences, The University of Tokyo, Kashiwa, Japan
[3] Meteorology and Glaciology Group, National Institute of Polar Research, Tachikawa, Japan
[4] Technical Research Center, Japan Marine United Corporation, Tsu, Japan

Abstract

The Japanese Antarctic research icebreaker *Shirase* has encountered severe ice conditions during her operations in the Antarctic sea ice. Ramming performance influences the voyage schedule and safe operation in heavy ice conditions. This paper presents a proposed method of calculating the penetration distance during ramming operations. Ship–ice collision, ship slide–up, and ice failure were modeled. Bending failure was applied to ramming icebreaking criteria. The penetration distance obtained using the proposed method was compared with those from ship trials in the Antarctic sea ice.

1. Introduction

The Japanese Antarctic Research Expedition (JARE) was begun in 1956. The Antarctic research icebreaker *Shirase* II has transferred cargoes and scientists to the Japanese Antarctic research station (Syowa station) since 2009. *Syowa* station is located in Lützow–Holm Bay, which is often covered with the multi-year ice (Sawamura, 2016). *Shirase* is therefore often required to ram the multi-year ice. Ramming icebreaking requires more operation time and fuel than continuous icebreaking. Therefore, ramming performance strongly affects Antarctic voyage schedules and safe operations (Yamauchi and others, 2009).

During ship ramming, the icebreaker repeats backward and forward motion and breaks the sea ice by ship–ice impact and slide–up of the ship onto the ice. To model ship ram events, the complicated ship–ice interactions during ramming must be described. Earlier studies related to calculation of ship ramming were conducted by Popov and others (1967) and Vaughan (1986). They have been cited by Dalay and Riska (1990). The calculations have assumed the ship–ice interactions during ship ramming to be the ship–ice impact problem. They have derived a simple formula of ramming force, in which energy conservation in modeling of ship ram is applied. Blanchet and others (1990) have applied the energy conservation principle to represent the ship–ice impact and ship slide-up with and without the flexural response of ship during ship ramming. They calculated the kinematic energy of ship–ice interactions. Kishi and others (1997) used the energy balance model to predict the penetration distance of ship ramming based on measured and model test data. Ringsberg and others (2014) analyzed the relation between measured ship motions and ice loads. They proposed the computational

model to identify ramming force during ship–ice events in the heavy ice conditions. Takahashi and others (2019) investigated measured data of impact velocity, penetration distance, and turning angle of the icebreaker *Shirase*. They predicted the required time for turning operations of ship ramming. Use of the present predictions of ship ramming remains limited because most predictions require measured or model test data of ship ramming.

This paper presents calculation of the penetration distance of ship ramming based on energy conservation in ship–ice interactions of ship ramming. The phenomena of ship–ice impact, ship slide–up, and ship–ice friction are involved in the energy balance during ship ramming. Bending failure of plate ice is applied to the ship ramming icebreaking. The proposed method calculates the penetration distance. Results were compared with the penetration distance of icebreaker *Shirase* measured in the 55th Japanese Antarctic Research Expedition (JARE 55) on 2013 and 2014.

2. Ship ramming in the Antarctic sea ice

Shirase conducted her operations in the Antarctic sea ice for the 55th Japanese Antarctic Research Expedition (JARE 55) during December 2013 through March 2014. During the outbound voyage to *Showa* station, *Shirase* started her ramming operations from December 18, 2013, when she entered the multi-year ice (69°00'N, 39°05'E), and continued until January 4, 2014 when she berthed at *Showa* station (69°00'N, 39°38'E). The ramming in multi-year ice was done 1952 times. *Shirase* is equipped with a ship-monitoring system that records ship motion data during her voyage (Yamauch and others, 2011). This paper used ship data related to the ramming, such as ship

speed, GPS location, ship power, ice thickness, etc.

2.1 Ice thickness

The ice thickness was measured by an electro–magnetic induction sensor (EM sensor) installed at the starboard shoulder. Visual observation and image analysis were also used for ice thickness measurements. Image analysis measures the ice thickness using the digital camera and laser measure. The digital camera captures the vertical cross section of ice when the ship breaks the ice and the ice is rotated by the ship advancing. At the same time, the laser measures the distance between the digital camera and the ice. The length of the 1 pixel's image is obtainable by the function with the distance from the digital camera to the ice. The ice thickness is calculated by the number of the pixels in the ice cross section and the length of the 1 pixel's image. (Sawamura, 2016). EM sensor can measure only the total sea ice thickness (snow+ice). Others can measure snow and ice thickness separately. The time interval of the EM sensor is 1 s, and others sensor frequencies are 3 hours. Image analyses during water flushing performance tests were conducted in each ramming. The time interval was varied from 5 to 10 min depending on each ramming operation. In the water flushing system, water pumps with nozzles at the bow flush the ice to reduce the friction between hull and ice. Water flushing was used on and off alternately during water flushing performance tests. Tests were conducted during 18:50 (UTC) on Jan. 3, 2014 and 3:07 (UTC) on Jan. 4, 2014.

Table 1 shows the average ice and snow thickness at for 2013/12/22–23 (Area 01), 2014/01/03–04 (Area 02) and the water flushing test (Area 03). The total sea ice thickness obtained using the three method show moderately good agreement. The tendency of the total thickness is that visual observations revealed the greatest thickness, the EM sensor obtained an intermediate result, and image analysis obtained minimal thickness. The average sea ice thickness on Feb. 22 and 23 in 2013 (Area 01) were about 5 m. The average thickness on Jan. 3, 2014 (Area 02) was about 4 m. The average thickness on Jan. 4, 2014 (Area 02) was about 3 m. In the water flushing test (Area 03), the differences of ice thickness among the three methods become larger than those in other areas (Area 01 and Area 02). The measured thickness during the water flushing test became approximately 2.5–3.5 m. The snow thickness during Feb. 22 and 23 in 2013 (Area 01) was greater than 1 m; during Jan. 3 and 4, 2014 (Area 02 and Area 03), it was less than 0.5 m. The measured data shows that the sea ice thickness gradually diminished as the days passed, which means the sea ice conditions in the early period of ramming operations were extremely heavy. Those in the end period close to Showa station were moderate.

Table 1. Measured ice and snow thickness　　Unit [m]

		2013/12 (Area 01)		2014/01 (Area 02)		Flush (Area 03)
		22	23	03	04	
EM sensor	Ice + snow	5.18	5.13	3.53	2.65	3.42
Visual observation	Ice	3.90	4.00	4.25	2.61	2.40
	Snow	1.50	1.42	0.23	0.29	0.23
	Ice + snow	5.40	5.42	4.48	2.90	2.63
Image analysis	Ice	3.98	3.10	3.12	1.96	2.02
	Snow	1.19	1.39	0.42	0.52	0.27
	Ice + snow	5.17	4.49	3.54	2.48	2.29

Table 2. Average value in one day of the maximum ship speed and thrust of each ship ramming

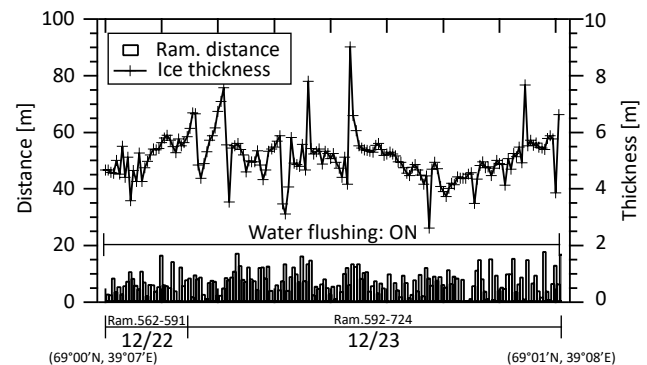| Date	Speed [m/s]	Thrust [kN]
2013/12/22	5.77	2068
2013/12/23	5.78	2338
2014/01/03	5.56	2168
2014/01/04	5.18	2156
Water flushing	5.31	2194

Fig. 1 Measured penetration distance and ice thickness on December 22 and 23, 2013 (Area 01, Ram. No. 562–724)

2.2 Penetration distance

The penetration distance of ramming is defined as the distance between arrival points of the present and preceding ram. The GPS data obtained from the ship-monitoring system were used to calculate the ship location. The GPS data were obtained every 1 s. The ship positions were accurate to around 10 m in GPS and around 7m in MSAS from the catalog data. Water flushing was done from December 18, 2013 to January 1, 2014. Moreover, water flushing was used during water flushing performance tests. Water flushing enables elongation of the ramming distance, especially for the ram with the thick snow. Table 2 shows the average value in one day of the maximum ship speed and thrust. The maximum ship speed and thrust of each ship ramming
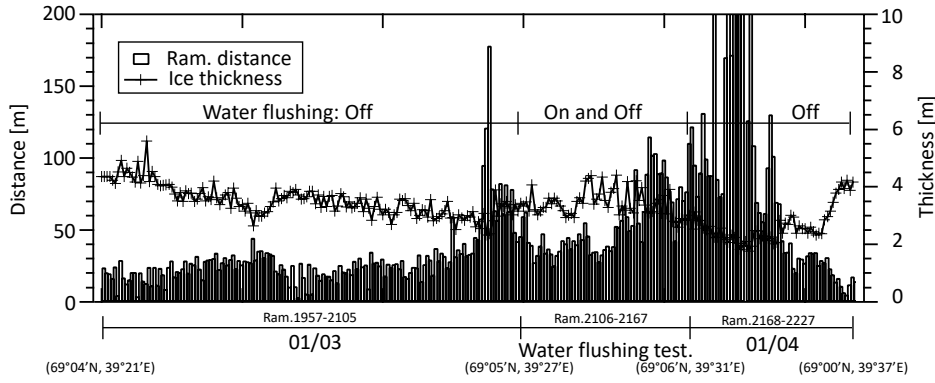
Fig. 2 Measured penetration distance and ice thickness on January 3 and 4, 2014
(Area 02 and Area 03, Ram. No. 1957–2227)

were unchanged during the ramming operations, which reveals the operational conditions were constant during ship ramming operation.

Fig. 1 portrays the measured penetration distance and the total sea ice thickness of each ramming in Area 01. Fig. 2 shows the penetration distance and the total sea ice thickness in Area 02 and Area 03. The total sea ice thickness measured by EM sensor was used in Figs. 1 and 2. In Fig. 1, the average penetration distance of one ramming is 7 m. The total penetration distance in Area 01 is 1187 m. In Fig. 2, the average penetration distance of one ramming is shown as 48 m. The total penetration distance Area 02 and Area 03 is 6978 m. The penetration distance in the heavy ice condition (Area 01) with total thickness greater than 4 m is extremely short; within 20 m. The penetration distance in the light ice condition (Area02 and Area 03), for which the total thickness becomes less than 3 m increases rapidly to longer than 100 m. Moreover, for sea ice thickness of less than 2 m, the penetration distance is greater than 200 m. Results demonstrate that the penetration distance is sensitive to the ice thickness. In Lützow–Holm Bay during December 2013 and January 2014, ice thickness of about 2 m apparently marked the transition from continuous to ramming icebreaking mode. For the short penetration distance within 10 m in the heavy ice conditions (Area 01), the accuracy of the ship positon obtained from GPS must be improved.

3. Method of ship ramming calculation
3.1 Energy conservation model

Vinogradov (Nozawa, 2006) proposed a formula to predict the maximum ice force during ship ramming based on the principle of energy conservation. Vinogradov's approach is as follows;

- The ship strikes the ice, and slides up on the ice using the kinetic energy and propeller thrust energy.
- The ice downward force increases with increase of gravitational force during the ship slide–up on ice.
- The kinetic energy and propeller thrust energy is expended in the ship–ice collision, potential energy and friction during the ship slide–up on ice.
- The ship breaks the ice when the ice downward force exceeds the ice breaking force before all available kinetic energy is expended.

The energy balance during ship ramming is expressed as;

$$(E_0 - E_1) + E_2 = E_3 + E_4 + E_5 \ , \qquad (1)$$

in which the following variables are defined.
E_0 = kinetic energy before ship ram
E_1 = kinetic energy after ramming icebreaking
E_2 = propulsive thrust energy
E_3 = energy dissipation of ship–ice collision
E_4 = potential energy of ship slide–up on ice
E_5 = energy dissipation of ship-ice friction.

$E_0 \sim E_5$ are expressed as shown below.

$$E_0 - E_1 = \frac{W}{2g}(v_0{}^2 - v_1{}^2)$$
$$E_2 = T \cdot S$$
$$E_3 = \frac{W}{2g}(v_0{}^2 \sin^2\phi)(1 - e^2) \qquad (2)$$
$$E_4 = \int_0^{Z_1} P_1 dz + \int_0^{\theta_1} P_1 q d\theta$$
$$E_5 = \frac{1}{\sin\phi}\int_0^{Z_1} F dz + \frac{1}{\sin\phi}\int_0^{\theta_1} F q d\theta$$

In those equations, v_0 represents the ship velocity before the ship ramming, v_1 denotes the ship velocity after ramming icebreaking, W stands for ship displacement, g is the gravitational constant, T denotes the mean propulsive thrust during ship ramming, S expresses the progress distance into the ice, ϕ signifies the stem angle, and e is the coefficient of restitution of the ship–ice collision. Z_1 represents the reduction of the average draft. Also, θ_1 is the change of trim angle during the ship ramming. P_1 stands for the vertical force at the ship–ice collision surface. F expresses the friction force on the

collision surface. The progress distance S and friction force F are expressed as

$$S = (Z_1 + q\theta_1)\cot\phi, \qquad (3)$$

$$F = f_\mathrm{i}\left(P_1\frac{\cos\phi}{\cos\beta} + T\frac{\cos\phi}{\cos\beta}\right).$$

Therein, the following variables are used:

$$Z_1 = \frac{P_1}{\rho A_\mathrm{W}g}, \qquad (4)$$

$$\theta_1 = \frac{P_1 q}{W \cdot KM_\mathrm{L}}.$$

In those equations, q denotes the distance between the ship–ice collision point and the center of floatation, β is the cosine of the frame angle, f_i is the coefficient of ship–ice friction, A_w represents the area of waterline, KM_L represents the height of longitudinal metacenter, ρ denotes the seawater density. Also, Eqs. 2–4 are substituted into Eq. 1, with the vertical ice force, P_1, expressed by Eq. (5).

$$P_1 = XT - \left[X^2T^2 + \frac{Y}{A}W^2\frac{v_0^2\{1-(1-e^2)\sin^2\phi\}-v_1^2}{gd}\right]^{\frac{1}{2}} \qquad (5)$$

In that equation, the following variables are used.

$$A = \frac{W}{\rho A_\mathrm{W}gd} + \frac{q^2}{KM_\mathrm{L}d},$$

$$X = \frac{1-\frac{f_i}{\cos\beta}\tan\phi}{1+\frac{f_i}{\cos\beta}\cot\phi}\cot\phi, \qquad (6)$$

$$Y = \frac{1}{1+\frac{f_i}{\cos\beta}\cot\phi}.$$

The ice is broken by ship ramming when P_1 is greater than the ice bearing force P_ice.

3.2 Ice breaking

Failure mechanisms by ship ramming are complicated. They include the local and global failure of bending, crushing, splitting, and flaking. Because few data have been collected on the behavior of icebreaking during ship ramming, the mechanism of the failure in ship ram has not been understood precisely. The analysis of this paper relied upon the simple assumption that icebreaking by ship ram occurs by local crushing on the ice edge and the bending failure of the plate ice.

At the points of ship–ice contact, ice crushing at the ice edge takes place as a ship advances in sea ice. The ice force increases concomitantly with increased crushing area of the ice edge. The ice force nominal to the collision surface, F_nom, is given as;

$$F_\mathrm{nom} = A_\mathrm{c}\sigma_\mathrm{c}, \qquad (7)$$

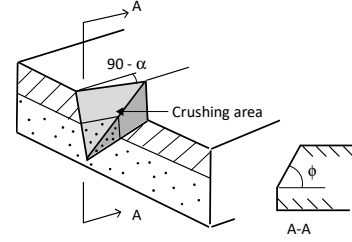where A_c represents the crushing area on the ship–ice
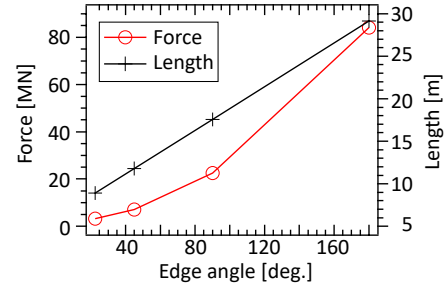

Fig. 3 Assumed stem and crushing area

Fig. 4 Icebreaking force and length calculated using FSI (force increasing rate = 10MN/s)

collision surface, σ_c denotes the ice crushing strength, which is called the mean value of crushing pressure by Kujala, 1994, and the average pressure by Daley, 1999. As the crushing area A_c increases, the crushing pressure σ_c decreases (e.g. Frederking, 2003, Frederking and Ritch, 2009). This crushing pressure-area relationship has scale dependency. For large contact area, the mean value of crushing pressure asymptotically approaches to a constant (Kujala, 1994). In this study, constant value of compression strength of ice is used as crushing pressure.

The crushing area, A_c, is calculated based on the collision geometry between the ship and ice. Daley (1999) calculated the nominal crushing area for different collision geometries (e.g. V wedge, symmetric spoon indentation, and right-apex oblique indentation) when he derived the force equation for ship–ice and structure–ice collision problems of ship ram. In this study, the collision between the wedge bow and 180° ice edge (V wedge indentation) was assumed. Reduction of draft Z_1 and change of the trim angle θ_1 were omitted from the calculation of A_c. Figure 3 depicts the crushing area by the geometrical relation between the stem and the ice edge.

The kinematic friction force is presented on the crushing surface. Coulomb type friction is assumed.

$$F_\mathrm{fric} = f_i F_\mathrm{nom} \qquad (8)$$

The total ice force normal to the collision surface is obtainable by the sum of the collision force F_nom and friction force F_fric. Ice crushing occurs until the crushing area increases and the downward ice force becomes sufficient to generate ice bending failure.

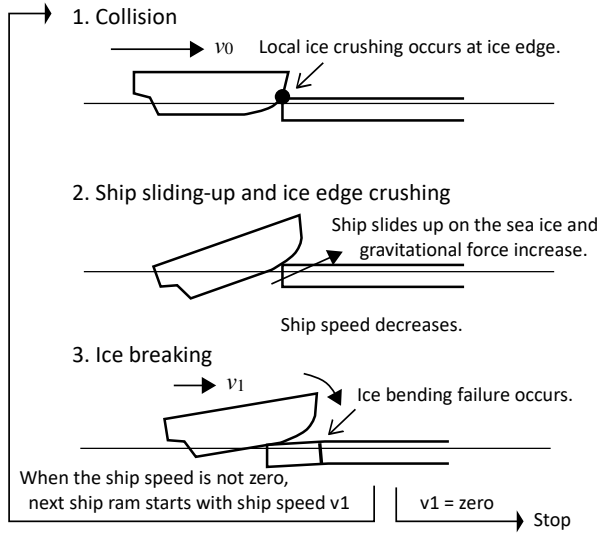Fig. 5 Ship ramming scenario

Bending failure of the plate ice occurs when the bending stress in the plate ice, σ_b, increases as the ship advances and exceeds the flexural strength of the ice, σ_f. σ_b is calculated using fluid–structure interaction (FSI) in which the dynamic effect of fluid underneath the plate ice is included along with plate ice bending (Sawamura and others, 2008). Ice bending in various ship–ice conditions (e.g. ice edge angle, thickness, and ship speed) is calculated using FSI. A database of the icebreaking force P_{ice} was prepared. In the ship ramming calculations for different ship–ice conditions, the icebreaking force is obtainable from this database (Sawamura and others, 2009). Figure 4 presents an example of database of plate icebreaking by ship ramming.

3.3 Ship ramming

A ship ramming scenario is idealized using the Vinogradov's approach. The ship ramming scenario is portrayed in Fig. 5. The penetration distance is calculated as described below.

- The ship strikes the ice edge with initial velocity v_0.
- The ship slides up on the sea ice. At the same time, the ice edge is broken by ice crushing.
- Ice downward force increases concomitantly with increase of the gravitational force that are created by the ice crushing and ship's slide-up.
- Ice bending failure occurs when the ice downward force P_1 exceeds the ice bearing force P_{ice}. The ship velocity decreases v_1 by the ship's slide-up and ice failure.
- The penetration distance S is calculated by the distance between arrival (ice breaking) points of the present and preceding ram. The total penetration distance S_{total} is calculated as the sum of each penetration distance S.
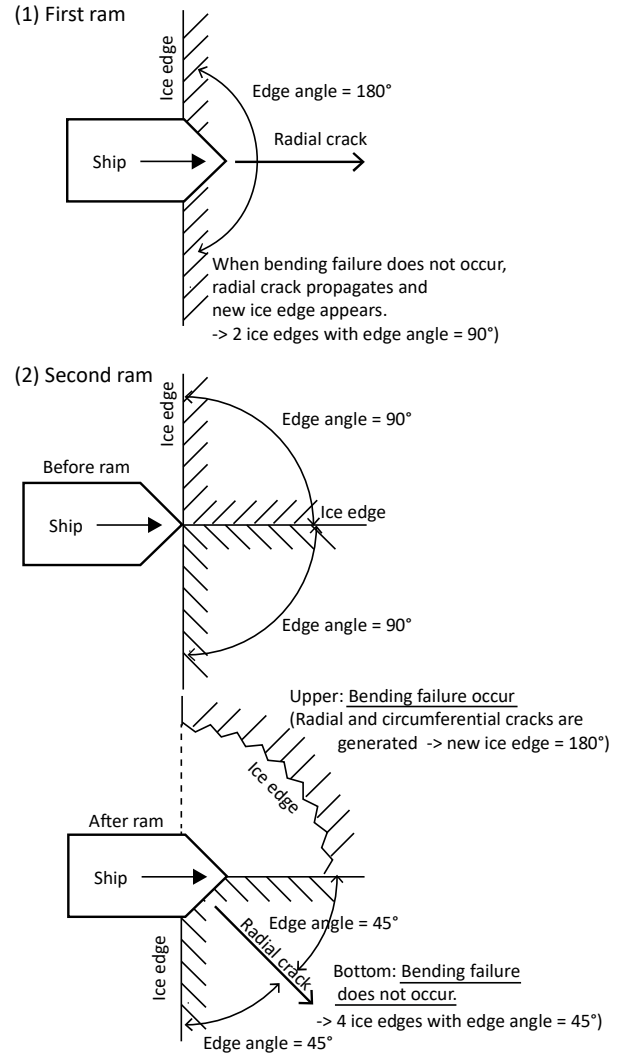

Fig. 6 Idealization of the radial and circumferential cracking of ship ram

The observations of the ship–ice interactions have revealed that ice failure begins by radial cracking starting from the ship–ice collision point, forming a circumferential crack. Ice breaks and falls off the plate ice by the penetration of circumferential crack. The calculations should include the effect of these cracks. In the calculations, when the ice bending failure is not occurred by the preceding ship ramming, only radial crack propagates. The ice edge is divided by the radial crack. The ice plate with two ice edges is generated, in which the edge angle is half size before preceding ship ramming. The ship ram starts for the plate ice with two ice edges. A schematic of ice breaking by radial and circumferential cracks is presented in Fig. 6.

4. Calculation of penetration distance

The measured ship speed, thrust, and the ice thickness were used for ramming distance calculations. The ship speed and thrust were measured respectively every 0.1 s and 1 s. In ship ramming, the ship speed decreases from

the maximum speed to zero as the ship moves through the sea ice. The maximum speed when the ship collides with the ice edge and the mean thrust during the ship ram (from maximum to zero speed) was used as the input data for calculations. The ice thickness measured by the EM sensor at zero speed when the ship ramming has just ended is used.

4.1 Mechanical properties of ice

The mechanical properties of sea ice were not measured in JARE 55. The flexural strength, however, is most important parameter of bending failure of ice. The flexural strength of multi-year ice in JARE 51 (Dec. 2009 – Mar. 2010) was estimated by the empirical formula using the brine volume of sea ice. The flexural strength at two locations in multi-year ice were 0.5 MPa and 0.8 MPa (Yamauch and others, 2011). For coefficient of restitution of sea ice, there is no available measured data. The coefficient of restitution obtained from the collision tests with pure ice block and ice sphere are available (Araoka and other, 1978). The coefficient of restitution of the pure ice was around 0.7.

The sensitive analysis are carried out for ice flexural strength and coefficient of restitution. The ice flexural strength from 0.3 MPa to 1.0 MPa and the coefficient of restitution from 0.0 to 1.0 are selected. Young's modulus, compression strength, and coefficient of friction of ice used in the model test of ship in level ice (Sawamura and others, 2016) are selected, because the flexural strength (0.5 MPa - 0.66 MPa) are similar values of those in JARE 51. The calculations were carried out for Area 01, Area 02, and Area 03. The principal dimensions of the icebreaker *Shirase* and the mechanical properties of the sea ice are presented respectively in Tables 3 and 4.

Table 3. Principal dimensions of icebreaker *Shirase*

Length of waterline	L_{wl}	126 m
Maximum width	B_m	28 m
Draft	d	9.2 m
Displacement		22000 ton
Bow angle		19 deg.

Table 4. Mechanical properties of sea ice

Young's modulus	E	300 MPa
Flexural strength	σ_f	0.5 MPa (0.3 MPa - 1.0 MPa)*
Compression strength	σ_c	0.7 MPa
Coefficient of Friction		0.1
Coefficient of restitution		0.7 (0 - 1)*

*Round brackets; for sensitive calculations

Table 5 and Table 6 show average of the calculated penetration distance using different bending strength (from 0.3 to 1.0 MPa) and coefficient of restitution (from 0.0 to 1.0). When the more than 10 times ramming

Table 5. Calculated penetration distance using different flexural strength (coefficient of restitution = 0.7)

Flexural strength [MPa]	1.0	0.8	0.7	0.5	0.3
Average [m]	5.87	7.73	8.84	12.4	16.1

Table 6. Calculated penetration distance using different coefficient of restitution (flexural strength = 0.5 MPa)

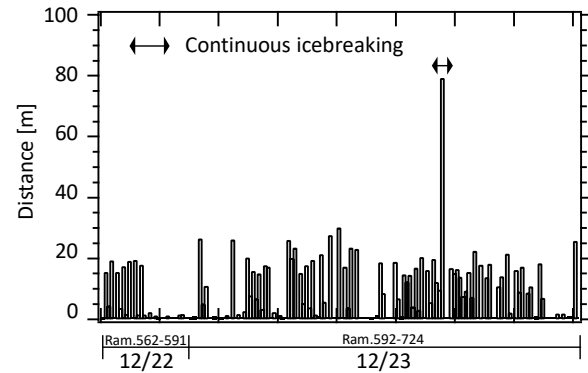| Restitution	1.0	0.8	0.6	0.4	0.3
Average [m]	12.7	12.6	12.1	12.1	12.0

Fig. 7 Calculated penetration distance on December 22 and 23, 2013 (Area 01, Ram. No. 562–724)

breaking are continued in one ship's ram, the calculation assumes the icebreaking to be continuous icebreaking instead of ramming icebreaking. From Table 5, and Table 6, ship ramming for icebreaking that was judged to be continuous icebreaking in the calculations was excluded. The average of the calculated penetration distance increase with increases of the flexural strength, but is unchanged by the coefficient of restitution. The average of the measured penetration distance was 22.7 m, which are larger than the calculated ones in Tables 5 and 6. Therefore, for the comparison of penetration distance (following subsection), the calculated results using the flexural strength of 0.5 MPa (the smaller one measured in JARE51) and the coefficient of restitution of 0.7 (the pure ice data measured by Araoka and other, 1978) are used.

4.2 Comparison of penetration distance

Fig. 7 portrays the calculated penetration distance for Area 01. Fig. 8 shows the calculated penetration distance for Area 02 and Area 03. The iterative calculation of ship ramming is ended when 10 consecutive ship rams are continued. For Area 01(2013/12/22–23), the calculated penetration distance of one ship's ram in the heavy ice condition (Fig. 7) is greater than the measured ones (Fig. 1). Some calculated penetration distances, however, become almost zero, for which only radial cracking occurs without the ice failure (circumferential cracking).
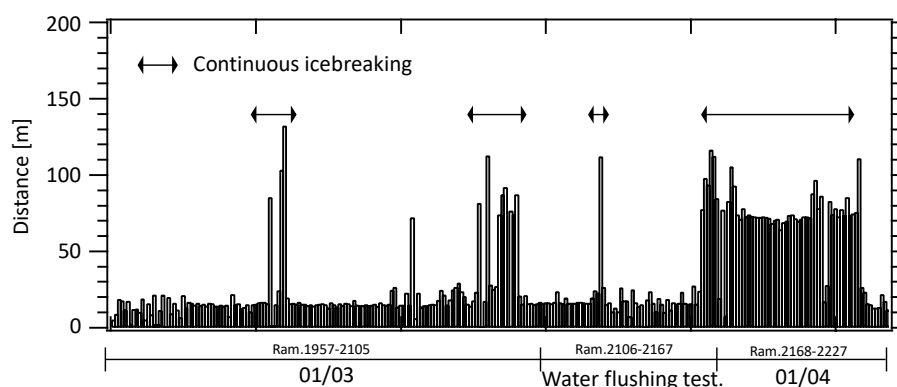
Fig. 8 Calculated penetration distance and ice thickness on Jan. 3 and 4, 2014
(Area 02 and Area 03, Ram. No. 1957–2227)

As shown in Figs. 1 and 7, distribution of the calculated penetration distance fluctuates more than that of the measured one.

For Area 02 and Area 03 (2014/1/03–04 and water flushing test), the calculated penetration distance of one ship's ram in the light ice condition (Fig. 8) is shorter than the measured ones (Fig. 2). In the calculations done for the icebreaking during Jan. 3, 2014 and in the water flushing test, the penetration distance was mostly constant: the penetration distance was about 20 m. For the calculations during Jan. 4, 2014, the continuous icebreaking continued instead of ramming icebreaking. As Figs. 2 and 8 show, the calculated distribution of the penetration distance was apparently more stable than the measured one.

Table 7 shows the total and average (standard deviation) penetration distance in one day, and the number of ship rams used for analysis of penetration distance. From Table 7, ship ram for icebreaking that was judged to be continuous icebreaking in the calculations was excluded. The calculated total penetration distance in heavy ice conditions (Area 01: 2013/12/22–23) moderately agrees with the measured values. The difference of the average penetration distance between measured data and calculated results are less than 2 m. The standard deviation of the calculated penetration distance in Area 01 is larger than that of measured one. The calculated penetration distance fluctuates more than that of the measured one in heavy ice conditions. The calculated total penetration distance in light ice conditions (Area 02 and Area 03: 2014/1/03–04 and water flashing test) was less than the measured values. The difference of the average penetration distance is around 10 m in Area 02 (2014/1/03–04), and around 17 m in Area 03 (water flushing test). The standard deviation of the calculated penetration distance in Area 02 and Area 03 are smaller than those of measured one. The calculated penetration distance was apparently more stable than the measured one in light ice conditions.

The snow thickness negatively affects the penetration distance. On the other hand, water flushing elongates the ramming distance. The measured penetration distance in the heavy ice conditions (Area 01: 2013/12/22–23) includes both effect of snow thickness and water flashing. Ice melted ponds were frequently distributed in Area 02 and Area 03 (2014/1/03–04 and water flushing test). The ice melted water reduces the friction between hull and ice, and elongates the penetration distance. In addition, the water flushing positively affects the penetration distance in Area 03. For the comparison with measured data, the calculation must include the effect of snow and water flushing. Yamauch and others (2011) investigated the snow and water flushing effect using the measured penetration distance in JARE 51. In the heavy ice condition with the ice thickness between 3 m and 4.5 m, the water flushing increased the penetration distance by 15% (around 7.5 m) regardless of snow thickness.

Table 7. Measured and calculated total, average (standard deviation) penetration distances and the number of ship rams (Top: total distance, middle: average distance, bottom: standard deviation)

Date	Measured ram [m]	Calculated ram [m]	Number of rams
2013/12/22 (Total, Avg., Std. dev.)	196	149	30
	6.76	4.97	
	3.61	7.23	
2013/12/23	991	1033	133
	7.51	7.77	
	4.26	8.69	
2014/01/03	3665	2139	136
	27.15	15.73	
	15.36	5.47	
2014/01/04	381	247	14
	27.25	17.64	
	30.81	5.59	
Water flushing test	2931	949	56
	53.30	16.95	
	22.25	5.31	

The penetration distance is strongly affected by the snow and water flushing. However calculations do not include effects of snow and the water flushing. For the calculations, the ice thickness and the mechanical properties of sea ice were assumed to be constant even when the real ship–ice conditions during ship ram were different. Only local ice crushing and global bending failure are included in the calculations as the icebreaking phenomena of the ship ramming. The propeller–ice interactions occurs normally in actual ship ramming, which reduces the propeller thrust, but they are not included in the calculations. Those problems are anticipated as reasons for the discrepancy between the calculated and measured values. They must be investigated and include in the calculation. The measured ship position is accurate to around 10 m in GPS. For the strict comparison, the more accurate data from the GPS data is needed.

4. Conclusions

This paper described the distributions of ice thickness and penetration distance of full-scale data. The calculation method of the penetration distance was proposed. In the calculations, the icebreaking by ship ram occurs by local crushing on the ice edge and the bending failure of the plate ice. The calculated penetration distance was compared with full-scale data for verification of the proposed method. The calculated penetration distance in heavy ice conditions (Area 01) moderately agrees with the measured values. Under light ice conditions (Area 02 and Area 03), the penetration distance of the calculations was shorter than those of measurements. From these results, the proposed method using bending failure as the breaking criterion in ship ramming can demonstrate the ice breaking of ship ram. However, the quantitative differences of the penetration distance between the measured data and the calculated results were shown. These discrepancies are expected to occur because of the neglect of the effects of water flushing, ice surface conditions such as snow and ice melted ponds in the calculations. Those effects must be included in calculations because the penetration distance is sensitive to ice thickness, snow thickness, and water flushing. The mechanical properties of sea ice, ship steering, cargo conditions, and so on also affect the penetration distance. To find the main contribution to the penetration distance from among them, the detailed investigation using the additional measurement data and the calculations should be done.

Acknowledgements

REFERENCES

Araoka. K., and Maeno. N. (1978) Measurements of Restitution Coefficients of Ice, Low Temperature Science, **A**, **36**, 55-65 (in Japanese).

Blanchet, B., H. R. Kivisid and J. Grinstead (1990): Equations for local ice energy dissipations during ship ramming. *Cold Region Science and Technology*, **18**, 101-115.

Daley, C. G. and K. Riska (1990): Review of Ship–ice Interaction Mechanics, *Report from Finnish–Canadian Joint Research Project No. 5 "Ship Interaction With Actual Ice Conditions" Interim Report on Task 1A*. Helsinki, Finland: Helsinki University of Technology.

Daley, C. (1999): Energy based ice collision forces, *Proc. of the 15th International Conference on Port and Ocean Engineering under Arctic Conditions*, **1**, 23-27.

Frederking, R (2003): Determination of Ice Pressure from Ship Transits in Ice, *Proceeding of the 13 International Offshore and Polar Engineering Conference*, **1**, 484-488.

Frederking, R and Ritch, R. (2009): The nature of the process pressure-area relation from CCGS Terry Fox berg bit impacts, *Proc. of the 19th International Offshore and Polar Engineering Conference*, 608-613.

Kishi, S. and Y. Kawashima (1997): Ramming Performance of the Patrol Icebreaker "PM TESHIO" in Full Scale and Model Scale, *Proc. of OMAE/POAC Joint Conf.*, **4**, 233-238.

Kujala, P. (1994): On the Statistics of Ice Loads on Ship Hull in Baltic, Mechanical Engineering Series, 116, Ship Laboratory, Helsinki University of Technology, Finland.

Nozawa, K. (2006): Sea ice Engineering: Seizando-Shoten Publishing Co. Ltd. Japan, 259-264 (in Japanese).

Ringsberg, J. W., M. Broman and P. Nordqvist (2014): Development of a Model for Global Response of Ship Hull during Ramming of Heavy Ice Features, *Proc. of the ASME 2014 33rd International Conference on OMAE*, OMAE2014-23186.

Sawamura, J., K. Riska and T. Moan (2008): Finite Element Analysis of Fluid–Ice Interaction during Ice Bending. *Proc. of 19th IAHR International Symposium on Ice*, 191-132.

Sawamura, J., K. Riska and T. Moan (2009): Numerical Simulation of Breaking Pattern in Level Ice at Ship's Bow, *Proc. of the 19th International Offshore and Polar Engineering Conference*, 600-607.

Sawamura, J. (2016): Ship–ice Interaction in Antarctic Sea. *Proc. of 23nd IAHR International Symposium on Ice*, USB.

Takahashi, Y., H. Yamaguchi and 3 others (2019): Turning features of an icebreaker during ramming operations: a case study. *Okhotsk Sea and Polar Oceans Research*, **3**, 13-19

Yamauchi, Y. and S. Mizuno (2009): Study on improvement in ramming performance of Antarctic icebreaker. *Proc. of the 19th International Offshore and Polar Engineering Conference*, 629-635.

Yamauchi, Y., S. Mizuno and H. Tsukuda (2011): The icebreaking performance of SHIRASE in the maiden Antarctic voyage. *Proc. of the 21st International Offshore and Polar Engineering Conference*. 1093-1099.